Validation of Numerical and Analytical Model of Bearing Type Bolted Steel Lap Joint with Friction-Slip Mechanism and a Threaded Portion of the Shank in Bearing

Rafał Budziński[1], Małgorzata Snela[2*], Lucjan Ślęczka[1]

[1] Faculty of Civil and Environmental Engineering and Architecture, Rzeszow University of Technology, Poznańska 2, 35-084 Rzeszów, Poland

[2] Faculty of Civil Engineering and Architecture, Lublin University of Technology, Nadbystrzycka 40, 20-618 Lublin, Poland

* Corresponding author's e-mail: m.snela@pollub.pl

ABSTRACT

The paper presents experimental investigations and numerical analysis of bearing type lap joint behaviour with one bolt and two shear planes joining thin-walled steel parts. The aim of the study is to describe the actual force-displacement F-Δ relationship for the tested joints and to represent it numerically by validated models with varying degrees of geometry detailing in the finite element analysis. Validation involves determining properties of plates, bolts and the entire shear joint based on individual experimental testing. The obtained shear characteristic include all main stages of F-Δ connection behaviour, as elastic phase, friction, slip and bearing. Although bearing joints are analysed, friction-slip mechanism resulting from tightening of the bolts is also examined. Analyses also take into account existence of threaded portion of the bolt shank in bearing. FEA model with bolt thread confirmed its validity in terms of predicting load-bearing capacity with an overestimation of 1% with respect to the experimental average. However, simplified cylindrical model of the bolt shank appeared to be more reliable in terms of initial bearing stiffness, where the value was 20% higher comparing to the empirical results. An analytical characteristic of the considered joint was also derived based on the component method, which required certain assumptions and adjustments to include the actual phases of connection behaviour. This approach provided a satisfactory match to the experimental results, characterised by underestimations of maximum force and initial bearing stiffness of 2.5 and 7.6% respectively.

Keywords: steel lap connection, finite element analysis, force-displacement relationship.

INTRODUCTION

Lap joints are commonly used in many steel structures, ranging from various framing systems to lattice structures. The main point in favour of these connections is the simplicity in manufacturing and assembly. This is due to the usually minimal or no effort involved in welding and the increased assembly tolerances caused by the bolt hole clearances. For these reasons they can provide sensible option for a number of applications. For hot-rolled structures, such arrangement is commonly used in fin plate connections [1] in order to constitute a simple joint. In certain types of structures, lap connections are the only reasonable solution from an economic and structural point of view. These include lattice transmission towers [2] or, in particular, thin-walled structures made of cold-formed members [3, 4]. The static response of these systems is highly influenced by the stiffness characteristics of the connections used, which means that particular attention must be paid to analysing their behaviour.

Steel members in cold-formed structures are usually connected by bearing type, lap joints – category A, according to EC3 [5]. The resistance of such connections remains the subject of research and analysis [6], but currently great

emphasis is placed on accurately determining the relationship between the load F and elongation Δ of the joint. Such F-Δ characteristic (or M-ϕ in case of moment resisting joints) is vital to predict real behaviour of such structures as steel lattice towers [7] and portal frames [8] and many others, so work on determining them is still ongoing.

Usually, in case of axially loaded bearing joints, general F-Δ can be predict as shown in Figure 1. One can distinguish three phases in their behaviour: the friction phase (AB in Fig.1), the sliding in the bolt hole phase (BC in Fig. 1), and the bearing phase (CD in Fig. 1) [9].

The actual response of the presented connection, however, involves the recognition of many phenomena or structural considerations. These include potentially low bearing resistance of thin walls, bolt hole clearance, tightening of the bolt, friction between components and the use of fully threaded or partially threaded bolts, but in such a way that the threaded part of the shank is in bearing with the edge of the bolt hole.

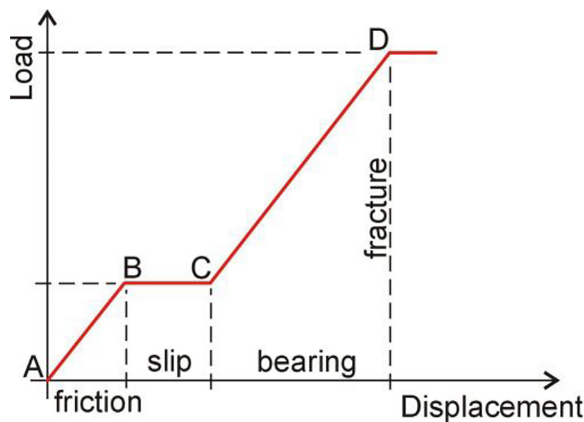Furthermore, Category A applies to non-pre-loaded bolts, with no tightening control. However,

there is in fact a certain torque, causing frictional response in the initial stage under minor loads. As frictional forces are overcome, another phase characterised by practically zero stiffness follows. It results from the aforementioned clearance in the bolt hole, which is intentionally designed according to the technical requirements [10]. This structural solution lead to a slip in the early phase of F-Δ relationship, resulting in increased elongation or rotation of the joints [8].

A load-bearing bolted connection exhibits intricate behaviour. First of all, because of the complex distribution within the connection due to the occurence of bearing and shearing action. These two phenomena combined lead to a resultant stiffness of the connection dependent on the bolt and steel components characteristics. Furthermore, the displacement of the lap joints can be attributed to the deformation of the hole, caused by the bolts exerting pressure on the thin walls of the connected components. It may be influenced by the presence of the threaded portion of the shank in the grip length of the bolt, therefore, a precise theoretical analysis is highly complex.

The design of bolted joints in the bearing can then be carried out using the empirical formulas available in the design guides [11] or the design codes. Consideration should be given to the EC3 standard [5], as its methodology enables predicting not only resistance, but also F-Δ relationship. This standard uses the component method to determine the contribution of each component in the developed joints. Each component of the joint is represented here by a spring for which the stiffness must be specified. The springs should be interconnected in a manner that replicates the behaviour of the analysed joint, enabling the determination of the properties of the analysed joint. As presented in Figure 2, several components shall be distinguished in the single shear
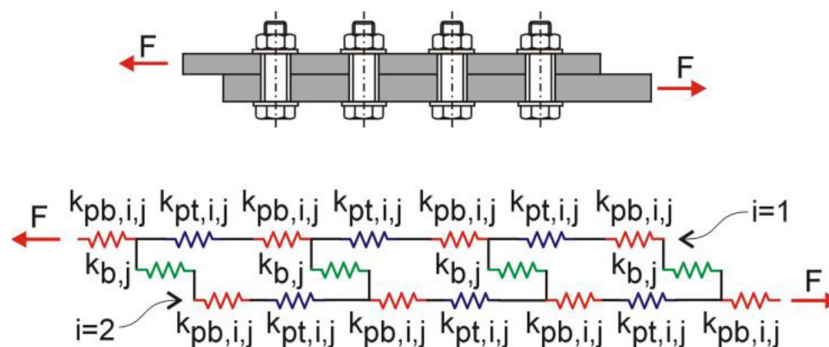

Figure 1. General load-displacement F-Δ characteristic for bolted lap connection

Figure 2. Mechanical model of the bolted lap joint based on the adapted component method

multi-bolt lap connection, including i-th plate in bearing ($k_{pb,i}$), i-th plate in tension ($k_{pt,i}$) and bolt in shear (k_b). In multi-shear connection the number of planes shall be also taken into account. In order to match the general trend shown in Figure 1, the k-coefficients of the presented components shall be considered separately in each j-th phase of the connections behaviour. In order to be able to derive this multilinear relationship, force limits shall also be defined for each stage. Similarly to the load-bearing capacity of the joint, the calculations of the slip resistance can be taken from the EC3 standard [5]. However, this requires some assumptions for the assembly conditions, which may be estimated based on recommendations of [10] and literature [12].

It is important to note that the Eurocode formulations, which were originally created for hot-rolled steel joints, may not be accurate, especially for cold-formed steel bolted joints. This has been demonstrated, among others, through numerical analyses conducted by Lee et al. [13] for the top-seat flange-cleat connection. Using numerical studies of bolted connections in cold-formed steel members, Chung and Ip [14] came to the conclusion that the design principles given in EC3 [5] are not relevant for bolted connections of high-strength cold-formed steel. This is primarily due to the decreased ductility of thin sheets. Furthermore, there are substantial discrepancies in the bearing capacities derived from the four established design principles. At the same time, there are studies demonstrating that the code model incorporated in EC3 enables an accurate prediction of the performance of joints in thin-walled structures [15]. Cai and Young tested the effects of end distance on thin sheet steel bolted connections. The test results were compared with the projected results obtained from the present design standards in terms of strength and failure modes. The reliability of the existing design guidelines was assessed by reliability analysis. In general, it was found that the EC3 specifications generally provide conservative predictions.

To predict the performance of joints in thin-walled structures, one can employ established models published in the literature. Many researchers have done studies and proposed different models that explain the behaviour of joints in structures with thin-walled sections. Kitipornchai et al. [16] introduced a theoretical model, based on Ramberg-Osgood type, to explain a continuous process of slippage. Ungkurapinan et al. [17]

conducted a series of experimental investigations on the slippage process of various types of bolted joints. They also constructed joint slippage models based on these experiments, which are represented by piecewise polynomial equations. The model created by Ungkurapinan served as the basis for later models. Zhan et al. [18] introduced an enhanced joint-slip model for standard galvanised single-leg bolted connections, which was derived from empirical findings. Balagopal et al. [19] provided a simpler model for a bolted connection in a truss lattice tower. This model takes into account both the axial and rotational stiffness. The model is based on experimental investigations conducted at the component level, specifically on a lap joint with two bolts. This model is comparable to Ungkurapinan's model.

In addition to models created based on the results of experimental tests, analyses were also carried out using numerical methods aimed at investigating the structural behaviour of thin-walled steel bolted connections. Different bolted connections in cold-formed steel structures subjected to shear loading have been investigated using finite elements models. Chung and Ip [20] developed a finite element model using three-dimensional solid elements to examine the occurrence of bearing failure in cold-formed steel bolted connections subjected to shear forces. Clamping forces created in bolt shanks, contact stiffness, and friction coefficients between element interfaces were considered as critical criteria for the precise prediction of the properties of bolted connections. Kim et al. [21] investigated how initial geometric imperfections affect the behaviour of cold-formed steel bolted connections. Gan et al. [22] introduced a methodology that uses the component method to predict the correlation between the load and deformation of the bolted connections. In addition, they applied the ABAQUS programme to construct FEM model. This model, along with their analytical model, was employed to acquire the desired correlations for two single-leg and two lap-splice bolted joints. Furthermore, the proposed analytical model was employed to forecast the relationship between load and deformation in a real-scale test. The projected results closely matched the findings of the experimental tests. Finite element modelling of shear tab connections for cold-formed sections conducted by El- Hosseiny et al. [23] showed, among other things, that the effect of pretension in bolts should be examined more thoroughly. Sevinc and Taskin

[24] conducted a numerical analysis to examine the relationship between the parameters that influence joint capacity, namely the pretension force and the surface friction coefficient between the joining plates, and the variation in the bearing capacity of the joint. It has been observed that the pretensioning force and friction coefficient both increase the joint's capacity in a comparable manner. The results demonstrate that the bearing capacity of a slip-critical joint can be enhanced by applying roughening techniques to the friction surfaces of the plate.

Another case related to FEM modelling of bearing type bolted connections is an appropriate selection of input parameters. One of these is the material law for high-strength steel bolts, which may influence the connection capacities. The bilinear or trilinear relationship proposed in a number of papers [25–27], based on nominal values, may not be satisfactory due to the underestimation of ultimate strength or ductility. The most reliable approach is based on experimental validation of the stress-strain function, which is efficiently performed, especially in connections with fasteners in tension. Results presented by Ostrowski [28] and Hu et al. [29] show, that the true material law may vary, especially for high-strength bolts. When it comes to bolts in shear, the validation of the bolt material appears to be more problematic. Although the analytical formula for bearing and shear resistance provided by the standard [5] is based on the ultimate strength, it is adjusted by empirical factors. In this regard, the applicability of the tensile stress-strain curve for shear cases might be considered under the condition of experimental verification. The complexity of modelling bolts in shear and bearing increases when it comes to the geometrical representation of the shank. It is especially important when the shearing plane passes through the threaded part of the fastener. It is usually simplified in the form of a cylinder with a cross-sectional area corresponding to the bolt core A_s. Nevertheless, it could potentially reduce the overall capacity of the connection, as presented by Ahmed et al. [30]. On the other hand, thread modelling in a bearing contact with a flat wall may arise convergence problems and be computationally expensive due to the increase of elements. Last but not least, few publications on FE analyses of lap connections consider the physical hole clearance in the model [22, 31], which is essential in representing the actual elongation of the joint including the slip phase.

An analysis of the current literature reveals that the behaviour of bearing type bolted lap connections is complex, especially when it comes to thin-walled steel members with low bearing capacity. Design guidelines and specifications for cold-formed steel joints primarily focus on evaluating the individual load-bearing capability of the joint's components, rather than taking into account the overall structural properties of the joints as a whole. Numerous extensive studies have been conducted to analyse and create efficient connecting systems. Despite the existing knowledge on the structural behaviour of connections between thin-walled steel elements, additional research is still required in this field. The objective of this study is to observe real behaviour of bearing type bolted steel lap joints, under the influence of the friction-slip mechanism at the beginning stage and with use of bolts with threaded portion of the shank in bearing. Additionally, the second objective is to describe the actual force-displacement F-Δ relationship for the tested joints and to represent it numerically by validated finite element models. After being validated, such FE model can be used in future work for parametric analyses.

EXPERIMENTAL INVESTIGATION OF DOUBLE LAP SHEAR CONNECTIONS WITH SINGLE BOLT

Single bolt shear test specimens

Experimental testing of single bolt lap shear connections was conducted to determine force limits and stiffness for the various stages of connection behaviour. The tested connection was designed to transmit tensile forces from steel plates by shearing of the bolt and bearing of the walls of the components. The specimen was arranged to achieve 2 shear planes in the bolts shank using two 4 mm and one 10 mm plate pieces of nominal S355 steel grade. In order to make the specimen possible to fit to the machine grip from the side of two thinner plates, a two-bolt connection with similar bolts was used to bring the cross-section back to another 10 mm plate. The 4 mm parts were uncoated and no traces of surface treatment was noted. In contrast, a rough surface after sandblasting was observed on 10 mm plates. The shear connections were made with zinc-coated ISO 4014 M16 8.8 bolts with partially threaded shank. In the introduced arrangement, the two shear planes

passed through different shank cross-sections – the threaded and unthreaded part. All fasteners were installed with washers under both head and nut. Normal round holes were prepared in the plates with a clearance of 2 mm corresponding to nominal bolt diameter based on [10]. A total of 6 bolt shear specimens were tested. The geometry of the specimen is presented in Figure 3.

The connections were made as category A bolted connections, provided the load transfer through bearing and no preload on the bolts. Nevertheless, the fasteners under testing were assembled with identical controlled torque of 60 Nm, which was intended to simulate tightening by hand. The applied torque is approximately equivalent to 25% of the value for preloaded bolts. The two bolts from the other side of the specimen where assembled with 200 Nm torque.

The objective of the experimental study is to obtain a failure form characterised by full yielding of the plate material. Therefore, large edge distances were adopted in the direction parallel and transverse to the load to prevent block tearing or net section fracture. Single bolt connection arrangement may constitute an equivalent component for a moment resisting lap joints commonly used in cold-formed frame structures of medium and long spans. The calculated resistance of these joints results from bearing capacity [8], the development of which is not affected by the wall rupture. This case may also relate to simple lap connections widely used in hot-rolled steel framing systems that require significant ductility, e.g. in an exceptional design situation [32]. It shall be noted, that such approach neglects the variation in normal contact pressure between joined elements, which may appear in a multi-bolt arrangement with a preload [33].

Testing instrumentation and procedure

The test was performed in INSTRON 1200 kN JD1 testing machine. ARAMIS 2D system was used to optically measure the in plane displacements of the bolts and the external surfaces of the plates. In order to obtain force-displacement relation for the tested single bolt connection, a virtual extensometer was set based on the facet points obtained from the surface pattern on the specimen. The gauge length points were located symmetrically to the bolt on the 4mm and 10mm plates beyond the overlapped area, at a distance of 140 mm. In addition, another corresponding extensometer was set in the area of two bolts in order to observe potential slip of this connection. Loading was applied in a monotonic manner with a displacement rate of 1mm/min.

Experimental tests results

The experimental force-displacement response of the connections with both one and two bolts is presented in Figure 4. A number of properties was extracted for various phases of
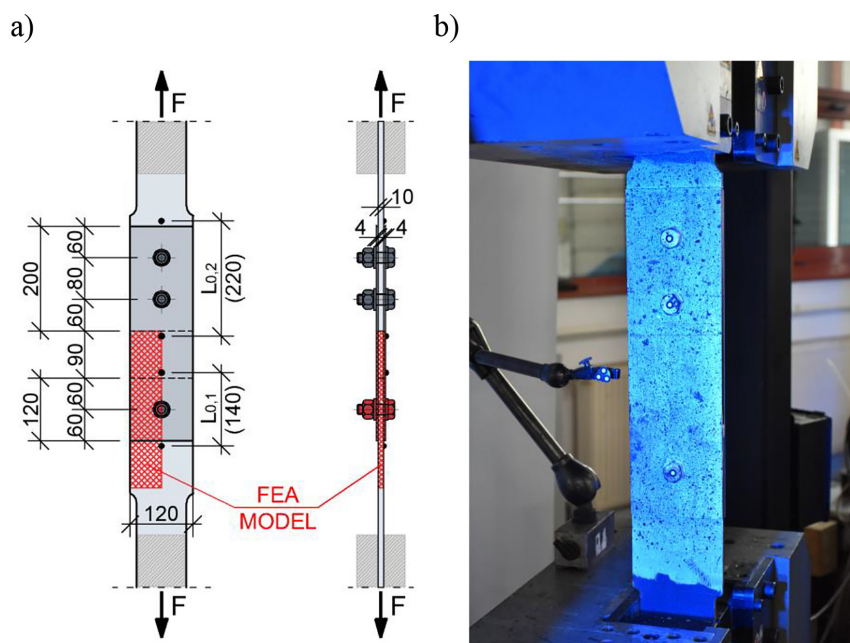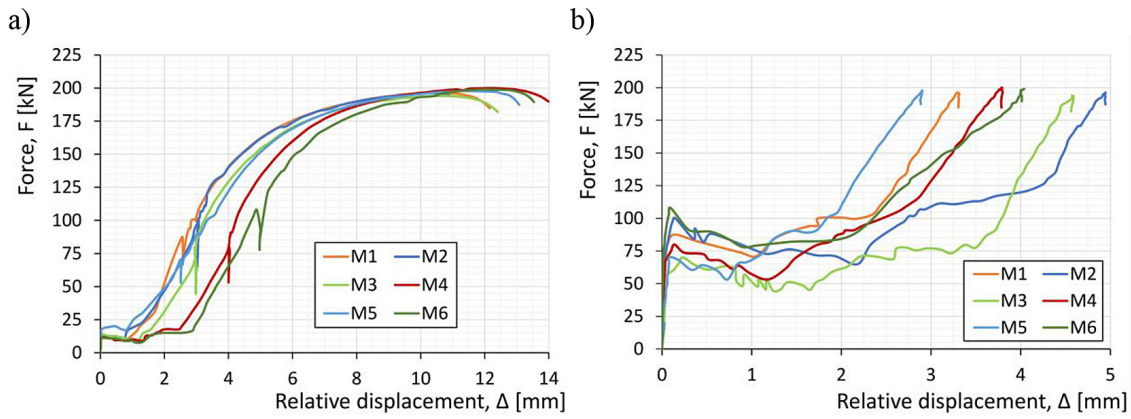

Figure 3. Tested specimen: a) geometry, b) a view of the testing stand

Figure 4. Force-relative displacement response (F-Δ) from experimental testing of a) single bolt and b) two bolts shear connections

the connection behaviour. Graphical explanation of determining these characteristics is shown in Figure 5. Some of the introduced properties limited to the initial bearing phase were also obtained for 2 bolted connections on the other side of the specimen. Mean values (MV) and coefficients of variation (CV) of these parameters for both types of connections are summarised in Table 1.

All single bolt connections demonstrated similar response considering force-extension curves. Due to small value of torque applied to
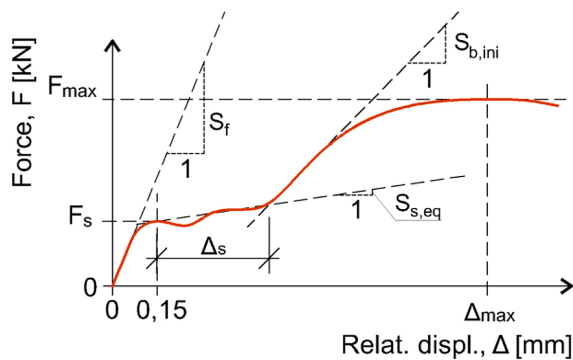
Figure 5. Graphical explanation of determining mechanical parameters from shear bolted specimens

the connections a relatively short frictional phase characterised by high stiffness was observed. Consequently the initial slip of the connection occurred at rather minor value of loading. The overall length of the slippage varied because of the random initial location of the bolt shank in relation to the holes. A slight stiffening during this stage was noticed, which is described by the equivalent stiffness value. The beginning of bearing contact appeared with a sudden increase in stiffness, which can be described by a linear relation. Further load growth induced flattening of the relation, leading to a yielding stage. After reaching maximum force the specimens did not show significant postcritical ductility and failed due to shearing of the bolt shank.

The connections with two bolts located on the other side of the specimens showed stiff friction phase throughout most of the test duration. By the end of the test, bolt slippage occurred in these connections and a friction phase was initiated. Based on this, the slip force results for these connections were extracted to extend the number of results for the determination of the friction coefficient for the tested arrangement. Coefficients

Table 1. Experimental results of double lap shear connections

Type of connection	No. of specimens	Distribution param.	Max. force $F_{max,exp}$	Slip load $F_{s,exp}$	Exten. at max. force $\Delta_{max,exp}$	Length of slip stage $\Delta_{s,exp}$	Stiff. of friction stage $S_{f,exp}$	Eq. stiff. of slip stage $S_{s,eq,exp}$	Init. stiff. of bearing stage $S_{b,ini,exp}$
		[–]	[–]	[kN]	[kN]	[mm]	[mm]	[kN/mm]	[kN/mm]	[kN/mm]
1 bolt	6	MV	197.39	14.04	11.22	1.88	1027.9	5.7	43.7
		CV [%]	1.1	19.5	6.8	31.8	38.5	62.0	26.8
2 bolts	6	MV	–	86.89	–	2.80	684.2	10.7	103.5
		CV [%]	–	20.4	–	32.1	26.7	50.1	24.5

of variation of the introduced parameters showed comparable values in both types of connections. Slip loads are obviously different in each arrangement due to the number of bolts and applied torque. The stiffness values for slip and bearing stage were approximately 2 times larger for the connection with two fasteners. In the case of the friction phase, this relation appears to be the opposite in favour of the single-bolt connection.

EXPERIMENTAL INVESTIGATION OF MECHANICAL STEEL PROPERTIES OF PLATES AND BOLTS

Tensile testing of pieces from steel plates

Basic tensile testing was performed on flat test pieces taken from 4 mm and 10 mm parts of nominal S355 steel grade as specified in the standard [34]. A total of 6 specimens for each thickness group were tested. The experiment was conducted with a recommended force control in INSTRON 1200 kN JD1 testing machine. Stress and strain values were calculated based on force results from the testing machine and relative displacement obtained from optical extensometer, respectively. All the aforementioned mechanical steel properties of test pieces including their variations are summarised in Table 2.

Tensile testing of bolts

In order to properly model the behaviour of the introduced connections, the mechanical properties of high strength bolts steel were investigated on the basis of tensile experimental testing. In total, 6 specimens consisting of a M16 8.8 bolt and a nut

were tested. The bolt specimens were assembled without torque control by hand. The testing setup consisted of robust adaptors dedicated for tensile testing of the fasteners, adapted to the INSTRON 1200 kN JD1 testing machine. The tests were conducted with a displacement rate of 1 mm/min with a slope leading to 4 mm/min after reaching plastic range. Relative displacement of the specimen was registered by optical measurements using the ARAMIS 2D system, which was utilised as an extensometer. The aforementioned adaptors used in the testing stand severely limited the possibility to observe the specimen throughout its length. In this regard the gauge length was set between head and a nut which were visible through holes located in the adaptors. The tests results including mean values of ultimate force, relative displacement at ultimate force and initial stiffness together with variations are summarised in Table 3. The geometry and view of the testing stand is shown in Figure 6.

FINITE ELEMENT ANALYSIS OF DOUBLE LAP SHEAR CONNECTION

The objective of the numerical analysis is to present a hierarchical validation approach based on experimental results and to determine the appropriate material and geometry input parameters for the investigated connection. The numerical results presented in this paper were obtained in ANSYS 2020 R1 software.

Derivation of the material law of steel plates

In order to validate the material law for the steel plates, a numerical model of the flat test pieces previously tested experimentally was

Table 2. Mechanical properties of steel from flat test pieces for each thickness group

Thickness group	No. of specimens	Yield strength f_y		Ultimate strength f_u		Ultimate strain ε_u	
		MV	CV	MV	CV	MV	CV
[mm]	[–]	[MPa]	[%]	[MPa]	[%]	[%]	[%]
4	6	404.4	2.1	527.8	1.2	16.0	6.4
10	6	393.7	1.8	517.6	0.8	16.6	2.5

Table 3. Experimental results of tensile testing of M16 8.8 bolts

No. of specimens	Maximum tensile force $F_{u,exp}$		Relative displacement at max. force $\Delta_{u,exp}$		Initial stiffness $K_{ini,exp}$	
	MV	CV	MV	CV	MV	CV
[-]	[kN]	[%]	[mm]	[%]	[kN/mm]	[%]
6	140.4	3.3	1.76	6.2	596.2	29.1
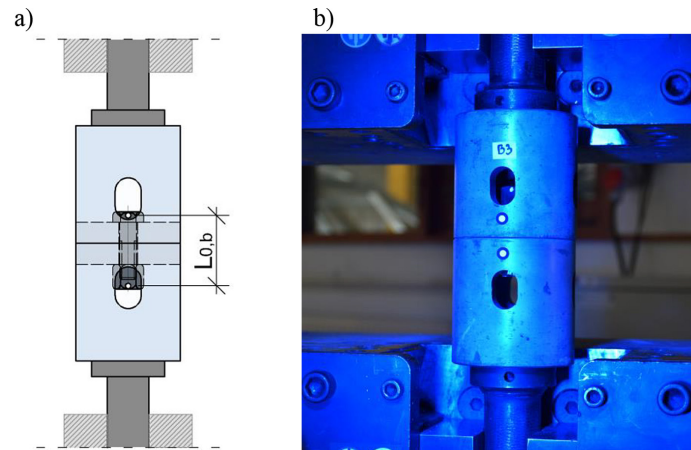
Figure 6. Testing stand: a) geometry view with the extensometer gauge length, b) actual view of the testing stand for tensile testing of bolts

prepared for both thickness groups. Thanks to the use of symmetry planes, models representing 1/8 of the geometry of the original sample were prepared. Frictionless supports were set on the 3 faces created in the cut-off planes. The loading was applied on the wider, gripped part of the test piece by displacement control. Hexahedral, quadratic order elements with 20 degrees of freedom (SOLID186) were used for the mesh. Five layers of elements were used throughout the thickness of the test pieces. The mesh was then adjusted to obtain elements with an aspect ratio close to 1. An extensometer with a similar gauge length to that used in the experimental studies was set up in the model. The material law for 4 mm and 10 mm thick specimens was adopted as a multilinear function built from experimental mean engineering stress values (σ) determined for strain (ε) increments of 0.0005 and 0.025 on the elastic and plastic region, respectively. These engineering values were then transformed into true stress σ_{tr} and strain ε_{tr} using the formulas:

$$\sigma_{tr} = \sigma(1 + \varepsilon) \tag{1}$$

$$\varepsilon_{tr} = ln(1 + \varepsilon) \tag{2}$$

Various approaches to the stress-strain curve for structural steel was compiled by Choung and Cho [35]. It was shown that experimental results based on force and displacement measures and transformed to true values are only accurate until ultimate strength is reached. The average relationship beyond this limit shall be retrieved through geometrical parameters collected from the necked area. However, when it comes to applying the material law to finite element analysis, it is important

to consider the equivalent true plastic stress-strain curve ($\sigma_{p,eq}$-ε_p). This relation may be described by the Swift's power law:

$$\sigma_{p,eq} = \sigma_{p,0} \left(1 + \frac{\varepsilon_p}{\varepsilon_{p,0}}\right)^n \tag{3}$$

where: $\sigma_{p,0}$ – initial true yield stress at hardening,
$\varepsilon_{p,0}$ – initial true yield strain at hardening,
n – plastic hardening exponent.

The plastic hardening exponent n is the slope of true plastic stress-strain function plotted on a natural logarithm scale:

$$n = \frac{d \ln(\sigma_p)}{d \ln(\varepsilon_p)} \tag{4}$$

The exponent value was evaluated from experimental data in the range from initial true yield at hardening to ultimate strength. Thanks to the presented formulas, the stress-strain curve was extrapolated beyond the above scope. This operation was performed in order to more reliably represent the necking stage of the test piece and the ductility of the eventual bolted connection model.

The force-strain relationship obtained from the finite element analysis of 10 mm test piece is presented alongside experimental curves in Figure 7. The comparison shows a satisfactory fitting of the numerical curve. Due to the adopted material law formulation, which is basic multilinear isotropic hardening, the curve shall be limited to the fracture point estimated from experimental data. A view of an exemplary test piece after fracture compared to the deformation of numerical model at predicted force limit is shown in Figure 8.
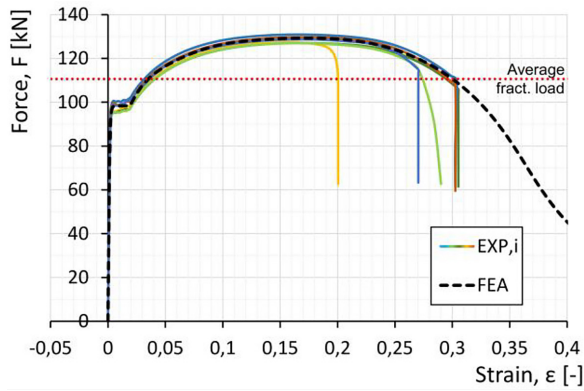
Figure 7. Force-strain response for 10 mm test pieces from experimental tests and finite element analysis

Derivation of the material law of high-strength bolts

The material law of high strength bolts was derived with the guidelines of the prEN 1993-1-14 [36], calibrated with the experimental results from tensile testing of fasteners. In order to verify the material model, a numerical analysis of the bolts in tension was conducted for various levels of geometrical representation of the threaded shank.

The experimental data extracted from the tensile testing of bolts did not allow direct transformation of the results to a stress-strain curve. In this regard, the material law was approximated based on the Ramberg Osgood model, which is among others dedicated to high-strength steels. The stress-strain (σ-ε) relationship is divided to two stages as follows:

$$\varepsilon = \begin{cases} \frac{\sigma}{E} + 0.002\left(\frac{\sigma}{f_y}\right)^{n'} & for\ \sigma \le f_y \\ \frac{\sigma-f_y}{E_{0.2}} + \left(\varepsilon_u + \varepsilon_{0.2} - \frac{f_u-f_y}{E_{0.2}}\right)\left(\frac{\sigma-f_y}{f_u-f_y}\right)^m + \varepsilon_{0.2} & for\ f_y < \sigma \le f_u \end{cases} \quad (5)$$

where: E – Young's modulus, f_y – yield strength (0.2% proof stress), f_u – ultimate strength, $E_{0.2}$ – tangent modulus at 0.2% strain presented in Equation 6, n' – coefficient

presented in Equation 7, $\varepsilon_{0.2}$ – corresponding total strain at 0.2% proof stress, ε_u – ultimate strain, m – second strain hardening exponent presented in Equation 8.

The tangent modulus at yield strength is defined by:

$$E_{0.2} = \frac{E}{1+0.002n'\frac{E}{fy}} \quad (6)$$

The coefficient appearing in the formula for strain within reaching yield stress is represented by:

$$n' = \frac{\ln(4)}{\ln\left(\frac{fy}{\sigma_{0.05}}\right)} \quad (7)$$

where: $\sigma_{0.05}$ – 0.05% proof stress.

The second strain hardening exponent occurring in the formula for strain stage between yield and ultimate strength is as follows:

$$m = \frac{\ln\left(0.008+\frac{\sigma_{1.0}-fy}{E}-\frac{\sigma_{1.0}-fy}{E_{0.2}}\right)-\ln\left(\varepsilon_u-\varepsilon_{0.2}-\frac{f_u-fy}{E_{0.2}}\right)}{\ln(\sigma_{1.0}-fy)-\ln(f_u-fy)} \quad (8)$$

where: $\sigma_{1.0}$ – 1% proof stress, $\varepsilon_{1.0}$ – corresponding total strain at 1% proof stress.

In order to apply this approach, it is necessary to determine several stress values at certain strain levels. Given the limited experimental results, some assumptions were made to estimate these values. With only the total elongation results for the whole tested bolt, it was assumed that the threaded part was responsible for all the plastic deformation. For the determination of the plastic engineering strain, the provisions of the standard for materials testing [34], specifically circular specimens, was suggested. The formula for the minimum parallel length, assumed to be equal to the free threaded length, was used to adopt the original gauge length. A Young's modulus of 210 GPa was assumed to complete the material description on the initial elastic range. The cross-sectional area of the bolt core A_s was considered as the reference value for the determination of engineering stresses. With these assumptions, it was possible to perform the material
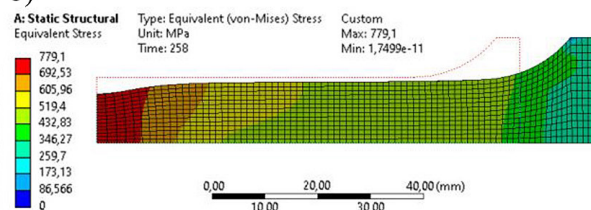
a)

b)

Figure 8. View of: a) exemplary 10 mm test piece after fracture, b) FEA model of 1/8 of the specimen at predicted fracture force

law approximation using Ramberg-Osgood model. The function was then transformed into true stress-strain relationship using Equations 1 and 2 and extended beyond the ultimate strength based on the power law approach presented in Equations 3 and 4.

The numerical analysis of the bolts in tension was performed on 4 different geometric representations of threaded portion of the shank: cylindrical with cross-section of bolt core A_s (V1), non-helical thread in the form of parallel transverse grooves (V2), helical thread with sharp edges (V3) and actual helical thread (V4). Geometric details including pitch and diameters of M16 thread was taken from ISO standards [37,

38]. A graphical presentation of all the analysed options is shown in Figure 9. Mesh visualisation of V3 bolt model is presented in Figure 10. The numerical model included head and nut, which were modelled in a simplified cylindrical shape. Bolt adaptors were omitted in the model. Fixed support and displacement were applied to the inner face of the head and nut, respectively. Cylindrical parts of the model were meshed using hexahedral, quadratic order elements with 20 degrees of freedom (SOLID186). Tetrahedral, quadratic order elements with 10 degrees of freedom (SOLID187) were used for the threaded parts of the shank in V2, V3 and V4 geometry variants. Global mesh of 2 mm size was refined to 1 mm
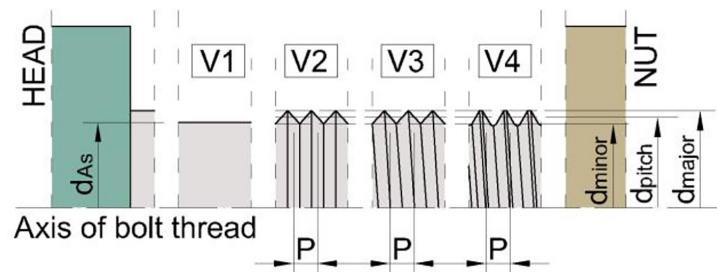

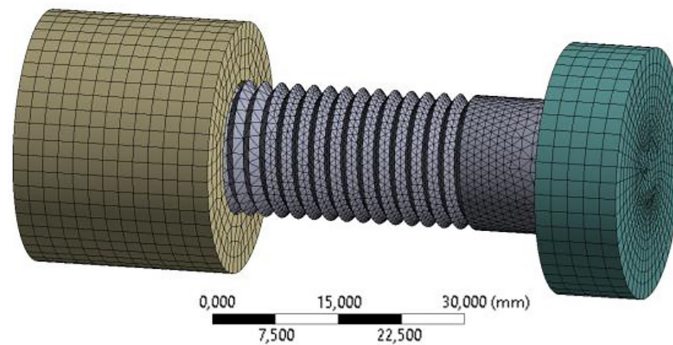**Figure 9.** Thread representation variants for the numerical model of bolt

Figure 10. Mesh view of V3 bolt variant model for numerical tensile simulation
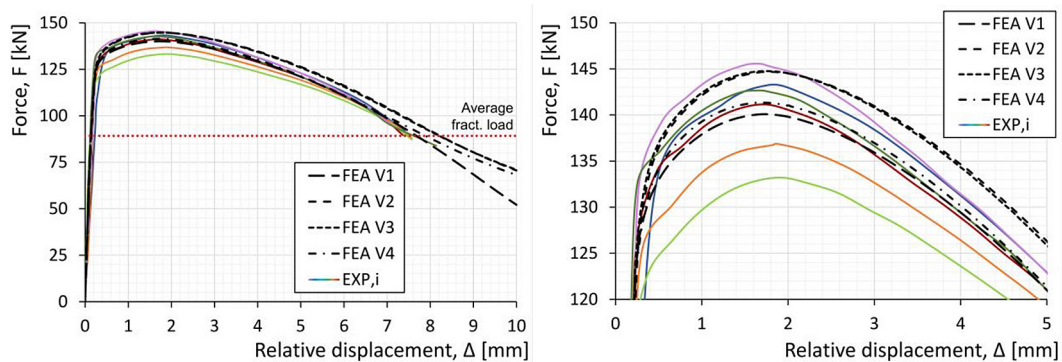

Figure 11. Force-relative displacement response for M16 8.8 test pieces from experimental tests and finite element analysis

on the bolt shank. An extensometer with a range similar to the experimental study, i.e. covering the distance from the head of the bolt to the nut, was specified in the model. The force-elongation relationship from the finite element analysis is shown alongside experimental curves from tensile testing of bolts in Figure 11. Similarly to the diagram related to test pieces from steel plates, average experimental fracture force is presented in order to set a possible limit for the numerical curve. A visual comparison of the exemplary experimental bolt specimen after fracture and the deformation of models at predicted force limit is shown in Figure 12. A summary of the results from finite element analysis of bolts in tension with reference also to the mean experimental values is presented in Table 4.

In general, the numerical responses presented adequate fit on both the positive and negative slopes, i.e. before and after the maximum tensile force is reached, respectively. In this case, the best global agreement was demonstrated by the V1 and V4 options. These variants were also the closest to estimating the maximum value of the force. In terms of the corresponding relative displacement, the V2 model proved to be the best fit. Larger deviations from the average test value were observed for the initial stiffness of the bolts. The numerical results show an overestimation of this parameter by 16–25%.
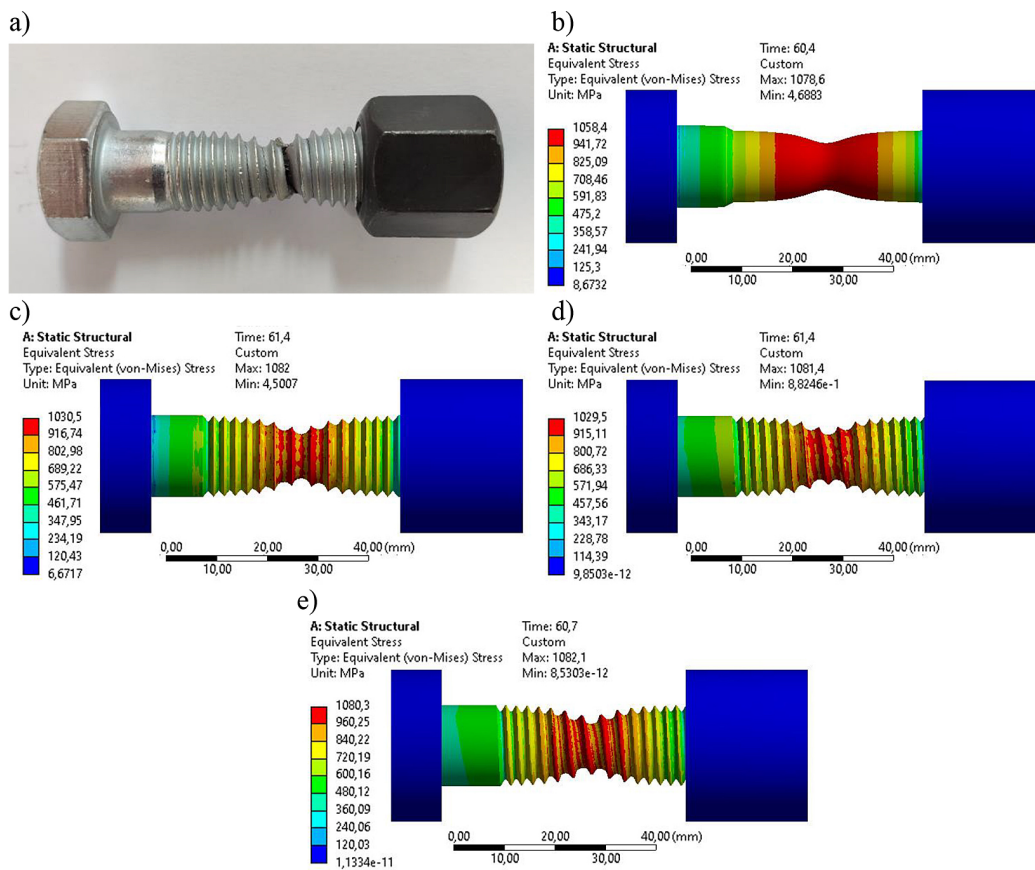

Figure 12. View of a) B5 bolt after fracture and b) V1, c) V2, d) V3 and e) V4 FEA models at predicted fracture force

Table 4. Summary of FEA results of bolts in tension

Variant of thread geometry	Ultimate force		Relative displacement at max. force		Initial stiffness	
	$F_{u, FE, i}$	$F_{u, FE, i}/F_{u, exp}$	$\Delta_{u, FE, i}$	$\Delta_{u, FE, i}/\Delta_{u, exp}$	$K_{ini, FE, i}$	$K_{ini, FE, i}/K_{ini, exp}$
[–]	[kN]	[%]	[mm]	[%]	[kN/mm]	[%]
V1	140.1	99.7	1.74	98.5	701.0	117.6
V2	144.7	103.0	1.77	100.7	696.2	116.8
V3	144.8	103.1	1.73	98.3	746.0	125.1
V4	141.4	100.6	1.69	96.1	724.2	121.5

Determination of frictional contact and bolt preload parameters

As presented earlier, even a small amount of tightening torque simulating hand tightening results in significant stiffening of the initial stage of bolted lap connections response under shear loading. The simulation of this phenomenon requires an estimation of friction parameters and bolt tension for the analysed case. The slip factor μ (coefficient of friction) relating to the shear planes between the steel plates was estimated from the experimental results for 1 and 2 bolts using the formula for slip resistance F_s [5] corresponding to the whole connection:

$$F_s = n_s \times \mu \times \Sigma F_p \qquad (9)$$

where: n_s – number of shear planes, ΣF_p – sum of the preloading forces from all bolts in the connection.

The preloading force in the bolt was determined from the general formula for tightening torque T [12]:

$$T = K \times F_p \times d \qquad (10)$$

where: K – torque factor, d – bolt diameter.

By transforming these formulas, assuming that the preloading forces are equal in all bolts, a direct formula for estimating the slip factor μ is as follows:

$$\mu = \frac{F_s \times K \times d}{n_s \times n_b \times T} \qquad (11)$$

where: n_b – number of bolts.

In order to correlate the preloading force to the bolt tightening torque, the torque factor K shall be determined. Since no detailed analysis was performed, an average value of 0.2 was assumed for zinc-plated bolts without lubrication based on [12]. Following that the mean values of coefficient of friction and preloading force were calculated on the grounds of experimental investigation of shear lap connections with 1 and 2 bolts. Finally, a slip factor μ equal to the global

mean value of 0.3605 was assumed. The results of this estimation are summarised in Table 5.

Frictional contact in the analysed connection also occurs between other parts, i.e. head and plate, nut and plate and bearing surfaces of shank and hole wall. All these cases involve friction of the untreated surface of the plates on the zinc-coated surface of the bolt or nut without lubrication. As no further investigation was conducted, a coefficient of friction value of 0.2 was assumed for the mentioned contacts based on a range of values corresponding to the presented conditions from the [39] guidelines.

Numerical model of double lap shear connection with single bolt

The numerical model of double lap shear specimen was reduced only to the part with the analysed connection with one bolt. The longitudinal range of the model geometry was adopted in order to cover the original base of the extensometer used in the experimental tests as presented in Figure 4a. The analysis was limited to only two variants of the bolt shank presented previously: V1 and V2. With these alternatives the model was also reduced to 1/2 of the original specimen taking advantage of the symmetry plane in the longitudinal direction. The bolt was placed centrally in the holes, which resulted in a clearance of 1 mm in both longitudinal directions. Similarly to the analysis of bolts in tension, the head and nut were modelled as cylinders. In this case, however, their heights were increased to simulate the presence of washers as they were omitted from being modelled as separate bodies. Therefore, the diameter of these components was assumed to be equal to the diameter of the washer due to the simulation of their frictional contact with the outer surfaces of the plates. Linear order elements were chosen in the analysis as they were considered more stable to achieve convergence of the bearing response beyond the models' capacity and less computationally expensive. The models were built using

Table 5. Summary of the estimation of friction and bolt preload parameters

Type of connection	No. of specimens	Torque T_i	Preloading bolt force $F_{p,i}$	Slip factor μ	
				MV	CV
	[–]	[Nm]	[kN]	[–]	[%]
1 bolt	6	60	18.75	0.374	19.5
2 bolts	6	200	62.5	0.348	20.1

hexagonal elements with 8 degrees of freedom (SOLID185). The exception was the threaded shank in V2 variant where tetrahedral elements with 4 degrees of freedom (SOLID285) were used. All parts involved in bearing and shearing action were meshed with layers of 1 mm high elements along the thickness of the plates and the longitudinal direction of the bolts. Moreover the mesh on the plates was refined in the area of the bolt holes and arranged in radially distributed layers. Fixed support were set to the 4 mm plates, while loading was applied through displacement control on the 10 mm plate. The cut-off faces of plates and bolt in the symmetry plane were given a frictionless type supports. The view of the numerical model of the connection is presented in Figure 13.

Numerical finite element analysis results

The numerical force-displacement response of the V1 and V2 models of the double lap shear connections with single bolt is presented alongside experimental curves in Figure 14. Both geometry variants showed similar response till reaching

bearing contact. High agreement of the slip force was observed compared to experimental testing. However, a certain deficiency was noticed in the stiffness of the initial frictional stage. The length of the slipping stage was negligibly larger than the total initial clearance of the bolt hole due to small penetration of the components. A discrete, secondary increase in the value of force in this range was observed. The initial stiffness at the bearing stage varied in both geometry variants. Although both models overestimated this characteristic, the V1 option with a cylindrical shank of A_s cross-section showed a more comparable response relative to the experimental results. The quantitative agreement of the results took the opposite trend in terms of the maximum load value. The V2 variant with non-helical thread overestimated this value by just over 1% compared to the mean experimental force. Finally, the V1 variant showed an accurate fit when considering the measured elongation at maximum load. The overestimation in this case was less than 1%. All the discussed values for both models are summarised with reference to mean experimental results in Table 6.
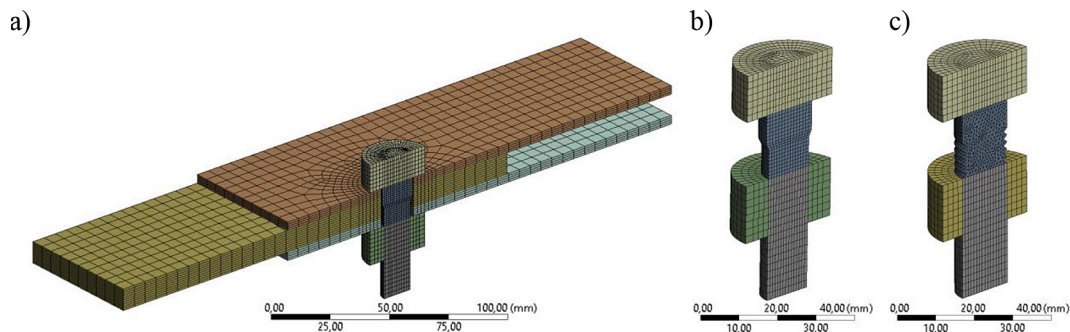

Figure 13. View of a) the 1/2 model of single bolt shear connection and meshing of b) V1 and c) V2 thread representation variant
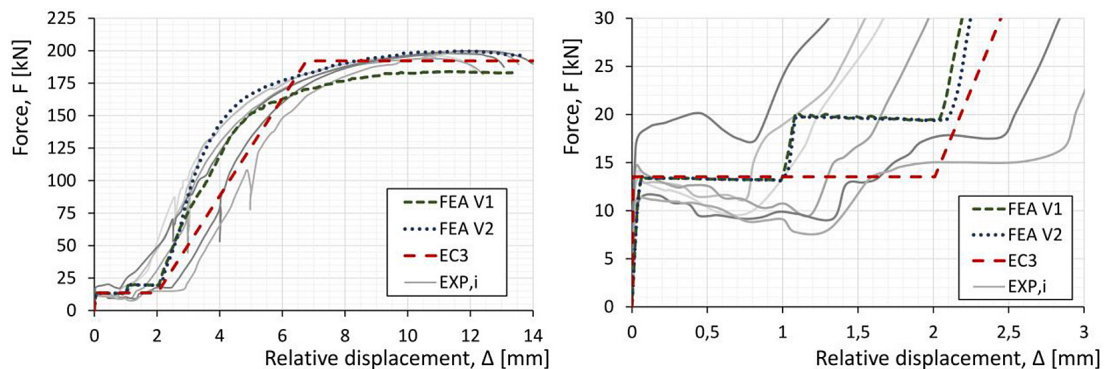

Figure 14. Force-relative displacement response (*F*-Δ) from numerical and analytical study alongside experimental results

Table 6. Summary of FEA and analytical results of double lap shear connections with single bolt

| Source of the results		Max. force F_{max}	Slip load F_s	Exten. at max. force Δ_{max}	Stiff. of friction stage S_f	Eq. stiff. of slip stage $S_{s,eq}$	Init. stiff. of bearing stage $S_{b,ini}$
		[kN]	[kN]	[mm]	[kN/mm]	[kN/mm]	[kN/mm]
FEA	V1	184.0	13.47	11.32	279.1	3.4	53.6
	V1/EXP [%]	93.2	95.9	100.9	27.2	60.1	122.7
	V2	199.6	13.48	11.92	277.5	3.4	74.2
	V2/EXP [%]	101.1	96.0	106.2	27.0	60.1	169.8
Analytical	EC3	192.2	13.52	–	1360	0	40.4
	EC3/EXP [%]	97.5	96.3	–	132.3	–	92.4
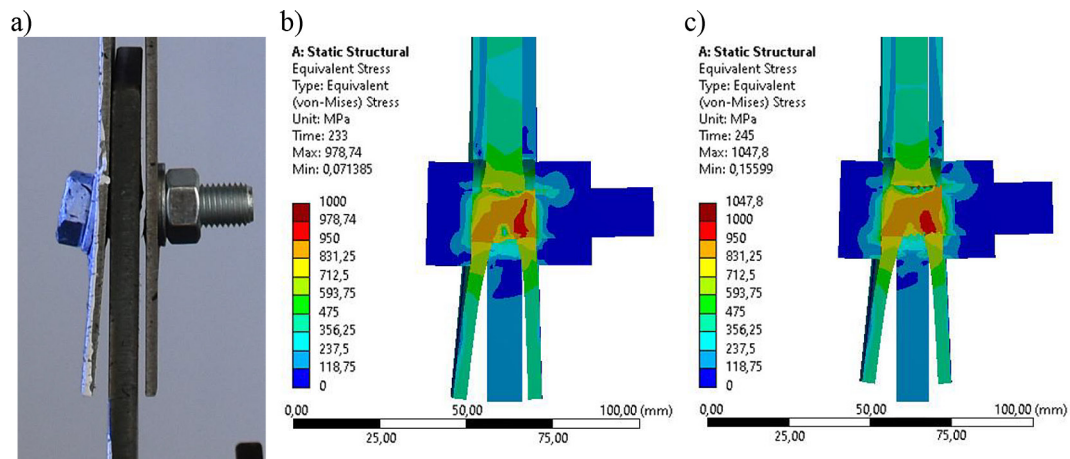
Figure 15. View of a) M5 shear specimen after fracture and equivalent stresses distribution for b) V1 and c) V2 FEA models at maximum load-bearing capacity
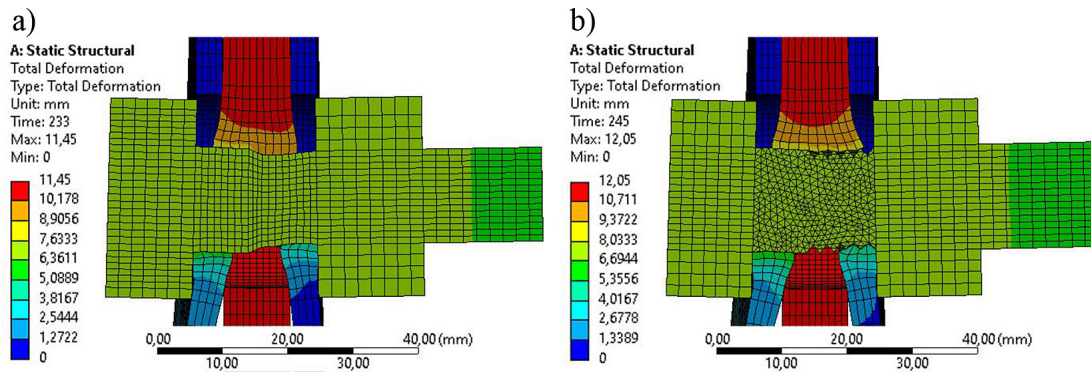
Figure 16. Deformation of shank and walls in bearing for a) V1 and b) V2 FEA models at maximum load-bearing capacity

Equivalent von Mises stresses for both bolt models at maximum force alongside a view of M5 specimen after fracture from experimental testing are presented in Figure 15. A close-up view of the deformation of the shank and the walls in bearing is shown in Figure 16. It can be observed that higher stresses were developed for V2 model, in which larger capacity was obtained.

The stress distribution and deformation of the model are comparable in both variants. The highest values occur in the threaded part of the cross-section in both variants. Piling of the material due to large yielding strain is observed on both the thick and thin plates in the hole area in each model. Mutual penetration at bearing contacts is observed only on the thinner plate side and the
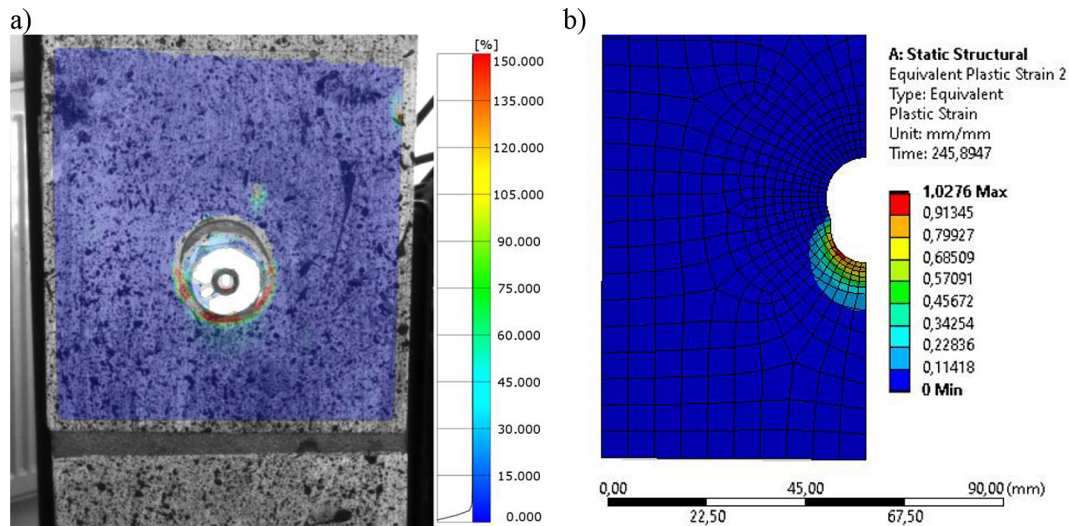
Figure 17. Total strain maps of a) M2 shear specimen from DIC optical measurements and b) V2 FEA model at maximum load-bearing capacity

threaded shank in the V2 variant. The contact on the thicker plate side is rather stiff, as no penetration is observed. A comparison of strain map on the outer face of 4 mm plate from M2 experimental specimen and V2 model at maximum force is shown in Figure 17. The highest values of plastic deformation accumulate within the sheet wall in bearing, as confirmed by experimental measurements made with the DIC optical measurements thanks to ARAMIS 2D system. The maximum strain values exceed 100% for both sources.

Discussion of the results

Numerical responses from the two geometry variants showed satisfactory agreement in relation to experimental study. Locally, some parameters even showed excellent compliance at the 1% level. This demonstrates the validity of the adopted approach in terms of derivation of material models, friction and bolt preload parameters. One difference that is noticeable when comparing the force-displacement curves is the discrete increase in force at the slip stage in the numerical responses. An analysis performed by the authors revealed that this is due to secondary slip between the head and nut and the outer surfaces of the plates. The greater the coefficient of friction is set for these planes, the greater the pitch observed on the relationship. Some stiffening along the slip range was actually noticed in experimental study (and represented by equivalent stiffness of slip stage $S_{s,eq}$), but in most cases it was more continuous than discrete. A certain deficiency that shall

be noted is the overestimation of the bearing stiffness for the V2 variant. As shown in Figure 16 b), the contact on the thread on the side of the thicker plate is rather hard due to the lack of penetration, which may contribute to a greater stiffness of the whole joint. A potential revision of the connection response at this stage may require further material validation in addition to the derived stress-strain curve or different contact formulation. In conclusion, the V1 model with a cylindrical shank on the threaded part represents a more accurate approach in terms of initial bearing stiffness while conservatively estimating the connection's resistance. In contrast, the V2 model with a simplified non-helical thread with parallel grooves exhibits an overestimation of stiffness at the similar stage, but shows an excellent representation of the ultimate load capacity.

Additionally, the 4 linear force – displacement relationship and several structural properties, derived from the adapted component method described in the introduction section, are also presented in Figure 14 and Table 6, respectively. The results of the analytical approach show an acceptable representation of the course of the joint response in relation to the experimental study. The assumed range and stiffness of friction and slip phase may be taken as correct for the initial A category connection performance. It shall be noted, that based on the analytical approach a more accurate estimation of frictional and initial bearing stiffness were obtained in comparison to finite element analysis. The ultimate capacity calculated as the sum of the shear resistances per plane,

assuming a full plastic redistribution of loading, resulted in a value 2.5% lower than the average experimental value. A certain deficiency in this approach is the lack of a hardening transition for the yield phase before full plastification and no estimation for the ductility parameter. The EC3 standard [5] does not provide such guidance, but there are publications that suggest certain solutions for estimating these parameters [9].

In general, the presented analytical method proved its accuracy for the prediction of the analysed lap connections performance. However, the comparison is based on only one specific case and should be extended to include variants with varying geometries, number and location of bolts and shear planes, and levels of bolt preload. It shall be also noted that the results in the current study were calculated based on actual average values obtained experimentally. Hence, the utility of the method may largely depend on the correct assumption of parameter values in the design calculations.

CONCLUSIONS

In this study, a finite element model of a bearing type bolted steel lap joint was built and successfully validated on own experimental results. The behaviour of considered bolted joint is influenced by friction-slip mechanism and, the existence of a threaded portion of the shank in bearing. Comparison between F-Δ relationships from test, finite element modelling and component method according to [5] was carried out. The conclusions include:
- The force – displacement (F-Δ) relationship obtained from FE modelling is very close to the dependence from the test for all represenations of the bolt geometry. Numerical model with the actual threaded portion of bolt shank showed an excellent match with regard to the load-bearing capacity of the joint, with a difference of only 1% compared to experimental tests. On the other hand, simplified cylindrical representation of the bolt shank appeared to be more accurate in terms of initial bearing stiffness with an overestimation of over 20% in relation to the empirical results.
- The analytical force – displacement polyline from the component modelling according to the adapted component method from [5] gives results close to the experimental and numerical

predictions. It is characterised by underestimations of maximum force and bearing stiffness of 2.5 and 7.6% respectively, compared to the experimental average.
- The influence of the threaded portion of the shank in bearing on initial stiffness of F-Δ curve (in post slip phase) is very little, at least in the case of the joint under consideration.
- Wider analyses are needed to confirm the possibility of using the component method to describe the F-Δ behaviour of bolted lap joints with thin sheets and the usage of fully threaded bolts. They can be performed as a parametric analysis using the validated FE model, described in the paper.

Acknowledgements

REFERENCES

1. SCI and BCSA. Joints in Steel Construction: Simple Joints to Eurocode 3. The Steel Construction Institute, 2014.

2. ECCS. Recommendations for Angles in Lattice Transmission Towers. ECCS Technical Committee 8, Brussels, 1985. http://www.eccspublications.eu.

3. TomàA, Sedlacek G, Weynand K. Connections in cold-formed steel. Thin-Walled Structures 1993; 16: 219–37. https://doi.org/10.1016/0263-8231(93)90046-d

4. Qin Y, Chen Z. Research on cold-formed steel connections: A state-of-the-art review. Steel and Composite Structures/Steel and Composite Structures 2016; 20: 21–41. https://doi.org/10.12989/scs.2016.20.1.02

5. EN 1993-1-8 Eurocode 3: Design of steel structures - Part 1–8: Design of joints. CEN, Brussels, 2006.

6. Draganić H, Dokšanović T, Markulak D. Investigation of bearing failure in steel single bolt lap connections. Journal of Constructional Steel Research 2014; 98: 59–72. https://doi.org/10.1016/j.jcsr.2014.02.011

7. Bernatowska E, Wojnar A, Ślęczka L. Behaviour of

steel lattice tower with partially preloaded bolted splices. Lecture Notes in Civil Engineering, 2023; 438: 13–21. https://doi.org/10.1007/978-3-031-44955-0_2

8. Budziński R, Ślęczka L. Experimental investigations of steel cold-formed moment-resisting bolted lap joints under monotonic and cyclic loading. Archives of Civil Engineering 2023. https://doi.org/10.24425/ace.2023.147664.

9. Henriques J, Jaspart J, Da Silva LS. Ductility requirements for the design of bolted lap shear connections in bearing. Advanced Steel Construction, 2014; 10(1): 33–52. https://doi.org/10.18057/ijasc.2014.10.1.3

10. EN 1090-2 - Execution of steel structures and aluminium structures - Part 2: Technical requirements for steel structures, CEN, Brussels, 2018.

11. ECCS, "European Recommendations for the Design of Simple Joints in Steel Structures", ECCS publication nº 126, Technical Committee 10, Structural Connections, Belgium, 2009.

12. Budynas, N, Richard, G., Nisbett K., Keith J. Shigley's mechanical engineering design. 10th Edition 8th Edition, McGraw-Hill Companies, New York, 2015.

13. Lee Y, Tan C, Lee Y, Tahir M, Mohammad S, Shek P. numerical modelling of stiffness and strength behaviour of top-seat flange-cleat connection for cold-formed double channel section. Applied Mechanics and Materials 2013; 284–287: 1426–30. https://doi.org/10.4028/www.scientific.net/amm.284-287.1426

14. Chung KF, Ip KH. Finite element investigation on the structural behaviour of cold-formed steel bolted connections. Engineering Structures/Engineering Structures (Online) 2001; 23: 1115–25. https://doi.org/10.1016/s0141-0296(01)00006-2

15. Cai Y, Young B. Effects of end distance on thin sheet steel bolted connections. Engineering Structures/Engineering Structures (Online) 2019; 196: 109331. https://doi.org/10.1016/j.engstruct.2019.109331

16. Kitipornchai S, Al-Bermani F, Peyrot A. Effect of Bolt Slippage on Ultimate Behavior of Lattice Structures. Journal of Structural Engineering 1994; 120(8): 2281–2287. https://doi.org/10.1061/(ASCE)0733-9445(1994)120:8(2281)

17. Ungkurapinan N, Chandrakeerthy S, Rajapakse R, Yue S. Joint slip in steel electric transmission towers. Engineering Structures/Engineering Structures (Online) 2003; 25: 779–88. https://doi.org/10.1016/s0141-0296(03)00003-8

18. Zhan Y, Li B, Wu Z, Cunningham L, Wu G, Yang Y. Modeling of galvanized lattice steel structures incorporating the effect of joint slip. Journal of Constructional Steel Research 2020; 173: 106252. https://doi.org/10.1016/j.jcsr.2020.106252

19. Balagopal R, Ramaswamy A, Palani G, Rao N. Simplified bolted connection model for analysis of transmission line towers. Structures 2020; 27: 2114–25. https://doi.org/10.1016/j.istruc.2020.08.029

20. Chung K, Ip K. Finite element investigation on the structural behaviour of cold-formed steel bolted connections. Engineering Structures/Engineering Structures (Online) 2001; 23: 1115–25. https://doi.org/10.1016/s0141-0296(01)00006-2

21. Kim T, Kuwamura H, Cho T. Prediction of ultimate behaviors in cold-formed steel bolted connection by the introduction of initial geometric imperfection in FE modeling. ISIJ International 2008; 48: 671–80. https://doi.org/10.2355/isijinternational.48.671

22. Gan Y, Deng H, Li C. Simplified joint-slippage model of bolted joint in lattice transmission tower. Structures 2021; 32: 1192–206. https://doi.org/10.1016/j.istruc.2021.03.022

23. El- Hosseiny OM, Ishac II., Maaly HM., Deebd MA.. Finite element study of shear tab connections for cold-formed sections, International Journal of Engineering and Innovative Technology (IJEIT) 2016; 5(7): 10–17. https://doi.org/10.17605/OSF.IO/ZBFKA

24. Sevinç S, Taşkin M. Numerical analysis of single lap pretension bolted joint. International Journal of Engineering and Applied Sciences 2023; 14: 77–90. https://doi.org/10.24107/ijeas.1218294

25. Hu Y, Davison B, Burgess I, Plank R. Multi-scale modelling of flexible end plate connections under fire conditions. Open Construction and Building Technology Journal 2010; 4: 88–104. https://doi.org/10.2174/1874836801004020088

26. Bahaari MR, Sherbourne AN. 3D simulation of bolted connections to unstiffened columns - II. Extended endplate connections. Journal of Constructional Steel Research 1996; 40: 189–223. https://doi.org/10.1016/s0143-974x(96)00049-1

27. Dessouki AK, Youssef AH, Ibrahim MM. Behavior of I-beam bolted extended end-plate moment connections. Ain Shams Engineering Journal/Ain Shams Engineering Journal 2013; 4: 685–99. https://doi.org/10.1016/j.asej.2013.03.004

28. Ostrowski K, Kozłowski A. Hierarchical validation of fem models of bolted joints. Journal of Civil Engineering, Environment and Architecture 2015; 32: 357–367. https://doi.prz.edu.pl/pl/pdf/biis/436

29. Hu Y., Shen L., Nie S., Yang B., Sha W. FE simulation and experimental tests of high-strength structural bolts under tension. Journal of Constructional Steel Research 2016; 126: 174–86. https://doi.org/10.1016/j.jcsr.2016.07.021

30. Ahmed A, Teh LH. Thread effects on the stiffness of bolted shear connections. Journal of Constructional Steel Research 2019; 160: 77–88. https://doi.org/10.1016/j.jcsr.2019.05.023

31. Liu X, Bradford M, Wang J. Load-slip behaviour of single-leg bolted angle steel connections at elevated temperatures. Structures 2022; 43: 1018–41. https://doi.org/10.1016/j.istruc.2022.07.014

32. Demonceau J-F, Golea T, Jaspart J-P, Elghazouli AY, Khalil Z, Santiago A, Santos AF, Silva L, Kuhlmann U, Skarmoutsos G, Baldassino N, Zandonini R, Bernardi M, Zordan M, Dinu F, Marginean I, Jakab D, Dubina D, Wertz F, Anwaar O. Design recommendations against progressive collapse in steel and steel-concrete buildings [FAILNOMORE]. ECCS - European Convention for Constructional Steelwork, 2021.

33. Grzejda R. Determination of bolt forces and normal contact pressure between elements in the system with many bolts for its assembly conditions. Advances in Science and Technology. Research Journal 2019, 13(1): 116–121. https://doi.org/10.12913/22998624/104657

34. EN ISO 6892-1:2009: Metallic Materials - Tensile Testing - Part 1: Method of a Test at Room Temperature, CEN, Brussels, 2009.

35. Choung J, Cho SR. Study on true stress correction from tensile tests. Journal of Mechanical Science and Technology 2008; 22: 1039–1051. https://doi.org/10.1007/s12206-008-0302-3

36. prEN 1993-1-14: Eurocode 3 - Design of steel structures - Part 1–14: Design assisted by finite element analysis, CEN, 2021.

37. ISO 68-1: ISO general purpose screw threads – Basic profile – Part 1: Metric screw threads, ISO, Geneva, 1998.

38. ISO 262: ISO general purpose metric screw threads — Selected sizes for bolts, screws, studs and nuts, ISO, Geneva, 2023.

39. VDI 2230-1 Systematic calculation of highly stressed bolted joints - Joints with one cylindrical bolt, VDI Verlag, Düsseldorf, 2015.